JOURNAL OF PROPULSION AND POWER
Vol. 9, No. 4, July–Aug. 1993

Thermal Nonequilibrium in a Low-Power Arcjet Nozzle

Dieter M. Zube*
Universität Stuttgart, Stuttgart, Germany
and
Roger M. Myers†
Sverdrup Technology, Inc., Cleveland, Ohio 44135

Emission spectroscopy measurements were made of the plasma flow inside the nozzle of a 1-kW-class arcjet thruster. The thruster propellant was a hydrogen-nitrogen mixture used to simulate fully decomposed hydrazine. Several 0.25-mm-diam holes were drilled into the 12-mm-long diverging section of the tungsten thruster nozzle to provide side-on optical access to the internal flow. Electron excitation for atomic species and molecular vibrational and rotational temperatures were determined for the expanding plasma using relative line ratio techniques. The atomic excitation temperature decreased from 18,000 K at a location 3-mm downstream of the constrictor to 9000 K at a location 9 mm from the constrictor, while the molecular vibrational and rotational temperatures decreased from 6500 to 3000 K and 8000 to 3000 K, respectively, between the same locations. The electron density, measured using H_β line Stark broadening, decreased from $\approx 10^{21}$ m^{-3} to 2×10^{20} m^{-3} during the expansion in the nozzle. The results show that the plasma is in a nonequilibrium state throughout most of the nozzle, with relaxation times close to or larger than the particle residence time.

Nomenclature

C	=	constant for calculating vibrational relaxation
E	=	excited state energy, J
E_H	=	hydrogen ionization energy, 2.18×10^{-18} J, 13.6 eV
f	=	oscillator strength
G	=	vibration excitation energy level, J
G_{eff}	=	factor used for calculating electron densities criterion for partial local thermal equilibrium validity
g	=	statistical weight, degeneracy
H	=	neutral atomic hydrogen
I	=	intensities integrated over the complete spectral line or band
K_2	=	constant for calculating vibrational relaxation
k	=	Boltzmann constant, 1.38×10^{-23} J/K
M	=	particle mass, amu
m	=	particle mass, kg
NI, NII	=	neutral and singly ionized atomic nitrogen
n_e	=	electron density, m^{-3}
P	=	protons, i.e., ionized atomic hydrogen
p	=	pressure, Eq. (6), MPa
T_e	=	electron temperature, K
T_{ex}	=	atomic electron excitation temperature, K
T_{rot}	=	rotational molecular temperature, K
T_{vib}	=	vibrational molecular temperature, K
z	=	degree of ionization +1, effective charge
$\ell n\,(\Lambda)$	=	coulomb logarithm[29]
λ	=	wavelength, nm
σ	=	cross sections, m^2
τ	=	relaxation times for temperature relaxation, s

Presented as Paper 91-2113 at the AIAA/SAE/ASME 27th Joint Propulsion Conference, Sacramento, CA, June 24–27, 1991; received Aug. 19, 1992; revision received Jan. 29, 1993; accepted for publication Feb. 17, 1993.

*Project Engineer, Institut für Raumfahrtsysteme, 7000 Stuttgart 80. Member AIAA.

†Propulsion Engineer, NASA Lewis Research Center Group. Member AIAA.

Introduction

SELECTION of a 1-kW class arcjet thruster for stationkeeping on the Telstar IV series satellites has dramatically increased interest in arcjet technology. The ability to achieve specific impulses from 450 to 550 s with storable propellants and the system simplicity made arcjets attractive for applications in geosynchronous satellite stationkeeping. Furthermore, modern satellite power buses have the capability to provide the required power/duty cycle combination for these thrusters. While arcjets have thus been accepted by the satellite community for geosynchronous stationkeeping, there is considerable room for improved thruster performance. Current arcjets convert only about 30–35% of the input power into thrust power, with considerable losses due to unrecovered power deposited into internal excitation of the propellant particles. This article describes an effort to empirically study the nozzle plasma conditions to obtain a more detailed understanding of the dominant plasma physics governing the thruster performance.

In a typical arcjet[1] an arc discharge is sustained between the central conical tipped cathode and the coaxial nozzle shaped anode. Propellant, injected near the cathode tip, passes through the throat (constrictor region) and is heated by various energy exchange mechanisms. Curran et al.,[2] using an axially segmented arcjet anode, showed that the anode current attachment extends all the way down the length of the nozzle. This result demonstrated that energy is transferred to the gas throughout the entire flow passage, including subsonic, transition, and supersonic flow regimes. The energy transfer from the arc to the gas is thought to be caused by electron-ion or electron-neutral collisions since electrons are the dominant current carriers. The energy is then distributed between the species by heavy particle collisions.

In addition to the directed kinetic energy, these collisions distribute the energy into several interval "sinks," including random thermal energy of the propellant, dissociation, ionization and excitation of rotational, vibrational and electronic states. Energy deposited into these modes constitutes one major loss mechanism for the arcjet thruster. While an analytical understanding of these processes is clearly required, the complexity of the flowfield and the plasma physics involved presently preclude an ab initio approach. To provide improved insights into the internal arcjet flows, efforts were

initiated to develop the diagnostic techniques required to directly measure several plasma parameters.

Most studies of arcjet plasmas have concentrated on the thruster plume. Studies utilizing langmuir probes[3,4] and emission spectroscopy[5] have established electron density and temperature profiles and identified the dominant species in the plume downstream of the exit plane. Several laboratories have developed and applied LIF techniques to the arcjet exhaust[6,7] as well as mass spectrometer measurements.[8] Janson et al.[9] found differences between the plume spectrum of an arcjet tested with ammonia and one tested with a nitrogen-hydrogen mixture chosen to simulate ammonia. While this indicates that the mixture used in this study to simulate hydrazine may not exactly represent a hydrazine arcjet, it should be noted that in a flight-type system, hydrazine is decomposed to a high degree in a catalyst bed before being injected into the arcjet, and performance comparisons[10] indicate only small differences between simulated and actual hydrazine propellants. The only previous study of the internal arcjet plasma was performed on a low power helium arcjet with a 2-mm-diam quartz constrictor.[11] However, due to the temperature restrictions of the quartz and the impact of the electrically isolating window section in the constrictor on the energy transfer processes in the constrictor, it would be unrealistic to relate their results to flight type arcjet thrusters.

The article presents the results of an effort to nonintrusively measure the plasma properties in an arcjet thruster similar to those planned for flight application. Following a description of the experimental apparatus and thruster operating characteristics, the measurements and their analysis are presented, including identification of the plasma constituents, atomic and molecular excitation temperatures, and the electron density. The results are then used to estimate various plasma relaxation rates. Finally, the implications of the results for plasma models are discussed.

Experimental Apparatus

The thruster used in this experiment was the 1-kW class laboratory device[12] that has been used extensively for arcjet diagnostics.[3-5,7] The thruster electrode/nozzle configuration was similar to that planned for application on geosynchronous communications satellites. The arcjet electrodes consisted of the typical conical-tipped, 2% thoriated tungsten cathode, a 0.64-mm-diam by 0.25-mm-length constrictor, and a conical nozzle/anode with an expansion angle of 20 deg and an area ratio of 1:225. Additional testing was performed with a nozzle expanding to an area ratio of 1:400 (same expansion angle). The anode material was 2% thoriated tungsten and all insulators were made of boron nitride.

The thruster was operated in a 0.64-m-diam by 0.64-m-length vacuum chamber evacuated by a mechanical roughing pump. The propellant flow consisted of a mixture of 5.95 mg/s hydrogen and 41.6 mg/s nitrogen to simulate fully decomposed hydrazine and was kept constant during all experiments [volume flow rate of 6 standard liters per minute (SLPM)]. With this flow rate the pump maintained an ambient pressure of about 120 Pa. This pressure, while affecting the plume shape, changed the thruster performance (thrust and voltage) by less than 5%.[10] The power supply[13] delivered a stable current that was varied between 9–12 A for the experiments. Thruster performance was measured on a thrust balance in a separate facility with higher pumping capacities described by Curran et al.[2]

Two optical diagnostic techniques[14] were developed to measure the emission spectra of the internal nozzle plasma. The more successful technique consisted of drilling 0.25-mm-diam holes into the nozzle wall at desired axial and radial positions to gain side-on optical access to the plasma inside the nozzle. As described in the next section, these holes had no measurable impact on thruster performance. Additionally, there was no evidence of preferential current attachment around the holes. The hole locations (Fig. 1) were chosen to provide measurements at three area ratios in the 1:225 nozzle and to obtain coarse radial profiles in both the 1:225 and 1:400 nozzles. The radial profiles were obtained at only one axial location ("C") with the 1:225 nozzle and two axial locations in the 1:400 nozzle. One axial location in this nozzle corresponded to the axial location "C" of the 1:225 nozzle, the other to the exit plane area ratio of the 1:225 nozzle. Assuming a radially symmetric distribution of the plasma in the nozzle, a simple Abel inversion technique was applied to the radial measurements, the solution was limited to $\frac{1}{4}$ the nozzle radius by the small nozzle size.

The optics required to image the individual holes onto the spectrometer entrance slit are shown in Fig. 2. The iris aperture was used to eliminate stray light emitted from the glowing nozzle wall. In order to select an individual hole, the thruster was moved vertically inside the vacuum chamber on

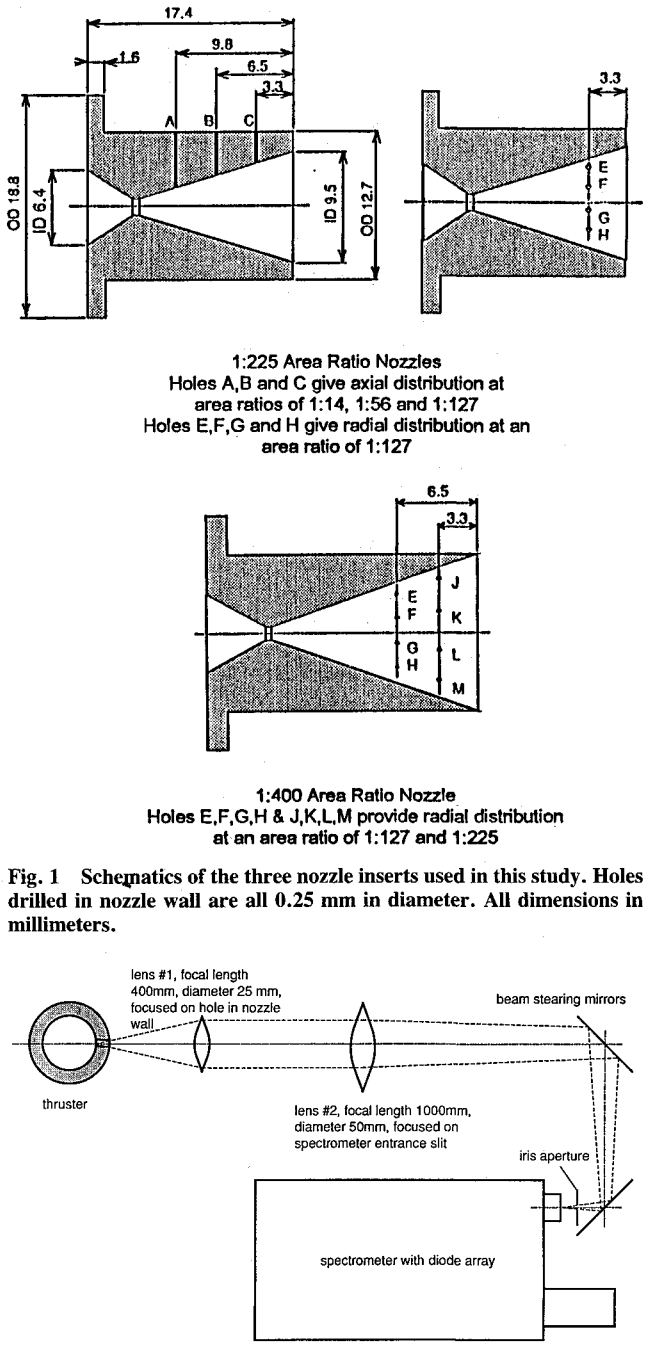

Fig. 1 Schematics of the three nozzle inserts used in this study. Holes drilled in nozzle wall are all 0.25 mm in diameter. All dimensions in millimeters.

Fig. 2 Optical arrangement used to image the holes in the arcjet nozzle walls onto the spectrometer entrance slit.

a stepper motor driven rail-table until the desired hole was at the source location of the light path.

The 0.5-m Czerny-Turner spectrometer was equipped with a 2400 grooves/mm holographic grating and an intensified 1024 pixel diode array detector to measure intensities. The spectral resolution of this instrumentation was 0.016–0.019 nm between two detector pixels, depending on the observed wavelength. Spectra were observed in real time to permit adjustment of the diode array integration time before storing them for later analyses.

Experimental Results

The current-voltage characteristic of the arcjet was obtained at the beginning of each measurement series to ensure the thruster was operating normally. Thrust measurements showed that the presence of the 0.25-mm holes in the nozzle wall had no measurable effect (<2%) on thruster performance. This was verified by testing the thruster with the holes both sealed and open. Excellent agreement was obtained with the life-test results reported by Curran et al.[12]

The measurements were hindered by light reflection from the nozzle wall opposite the holes, in addition to the optical system's complexity and small nozzle size. This issue is distinct from that of the glowing nozzle wall contributing continuum radiation, and is due to plasma luminosity reflecting of the inner nozzle surface into the holes through which measurement was made. This precluded the precise determination of the region where the light originated. The magnitude and origin of this light was defined by the nozzle geometry and surface reflectance. To establish the importance of this effect, a small light emitting diode (LED) was slowly shifted into the nozzle with the axial holes (configuration A in Fig. 1) and the light intensity emitting from the holes was measured as a function of LED location. For each hole there were two axial positions at which the LED provided a measurable signal: The primary location when the LED was directly beneath the hole and the secondary corresponding to the location that caused direct reflection from the opposite wall into the hole due to the 20-deg diverging angle of the nozzle. The secondary peak was brightest for the hole closest to the exit plane, but never exceeded 30% of the intensity of the direct illumination. It is important to note that this small test utilized a constant intensity source, whereas the plasma luminosity decreased rapidly in the downstream direction. While this intensity reduction reduced the importance of reflected light, it was not possible to exactly quantify the influence of this problem.

Whenever possible, the quantitative measurements utilized only spectral regions separated less than 40 nm to avoid the difficulties associated with intensities calibrations. For all measurements of steady-state conditions the thruster was turned on and allowed to stabilize for 15–20 min before a final alignment check was made to account for thermal expansion of the arcjet components. The uncertainties of the results were calculated by propagating the errors of the individual parameters using standard error propagating algorithms.[15]

Plasma Species

The plasma species identified from a spectrum recorded between 320–750 nm are listed in Table 1. Only species are reported for which several lines were identified. Observed wavelengths were compared with tabulations in Refs. 16–18. In addition to the molecular and atomic propellant species, tungsten (from the eroded electrodes), NH, and NH_2 lines were observed. The high NH intensities observed at all axial positions indicates that recombination was taking place throughout the nozzle. Nevertheless, NH spectral bands could not be utilized for temperature determinations due to a severe overlapping with N_2 spectral bands. Although the NH_2 and tungsten lines were visible in most experiments, their intensities were too low to use them for more detailed investigations.

Table 1 Identified species

Identified species	Identified wavelengths, nm
H	656.3, 486.1, 434.1
H_2	588.8, 587.9, 580.6, 577.5, 573.7, 572.9, 571.3, 565.6, 550.5
N	746.8, 744.2, 742.4, 584.1, 583.0, 575.3
N^+	571.1, 568.6, 568.0, 566.7
N_2	585.4, 581.5, 575.5, 559.9 larger bands at: 405.9, 399.8, 394.0, 385.8, 380.5, 375.6, 389.4, 388.9
N_2^+	586.5, 585.3, 556.4 bands at: 391.4, 388.4, 385.8
NH	bands at 336.0, 337.1, 450.1
NH_2	587.0, 570.7
W (Eroded electrodes)	584.5, 579.6, 579.3, 569.8, 566.1, 550.1, 412.5

Plasma Properties

The spectral data were used to determine several plasma temperatures and the electron density. The temperatures included the atomic excitation temperature for NI, NII, and H, and molecular vibrational and rotational temperatures for N_2. All temperatures were calculated assuming that the population of the observed excited states followed a Boltzmann distribution at the local temperature. The validity of this assumption was checked a posteriori. The results revealed that a Boltzmann distribution is valid for the population of the atomic species at least close to the constrictor, while the molecular species distribution seemed to deviate (details are discussed below).

Atomic Excitation and Free Electron Temperature

The apparent T_{ex} was determined from emission line ratios. This temperature can be calculated from two different lines denoted subscripts 1 and 2 of the same species[19]:

$$T_{ex} = \frac{E_1 - E_2}{k \ln(I_2\lambda_2^3 g_1 f_1 / I_1\lambda_1^3 g_2 f_2)} \quad (1)$$

The spectral lines used for this measurement are listed in Table 2, along with their oscillator strengths and the degeneracies of the upper excited states. A relative calibration was needed for the spectral response of the diode array detector for the hydrogen line measurements due to the wide wavelength separation of the observed transitions (H_α and H_β).

The axial excitation temperature distribution for NI, NII, and H for thruster operation at currents of 9 and 12 A with the 1:225 nozzle are shown in Figs. 3a–c. While the absolute uncertainties are large, most of them can be attributed to the uncertainties in the oscillator strength, which does not affect the validity of the observed trends. The excitation temperatures for the three species were similar, dropping from 18,000 K at an area ratio of 1:14 to 10,000 K at an area ratio of 1:127. The excitation temperature increased slightly with the arc current.

Radial electron excitation temperature profile measurements were made difficult by the rapid decrease in line intensities away from the nozzle axis. Only the hydrogen excitation temperature could be measured. The measurement was made at four radial positions in both the 1:225 and the 1:400 area ratio nozzles. The radial holes divided the nozzle section into four shells with an equal thickness of one-fourth of the radius. The Abel inversion technique used assumes a uniform intensity in each of the individual ring shells, and the intensity in a radial ring was calculated from the geometric size of the observed shell portion.[20] This simple technique was used because the small nozzle dimensions precluded measurements at a large number of radial locations. The measured spectra were inverted and the plasma properties were determined from these inverted intensities. As shown in Fig. 4,

Table 2 Transitions used to measure atomic excitation temperatures

Species	λ_{ik}, nm	f_{ik}	g_k
NI	583	0.00328	6
	583.4	0.00390	4
	585	0.00152	2
NII	566.7	0.339	5
	567.6	0.450	3
	568	0.380	7
H	656.3	0.6407	18
	486.1	0.1193	32

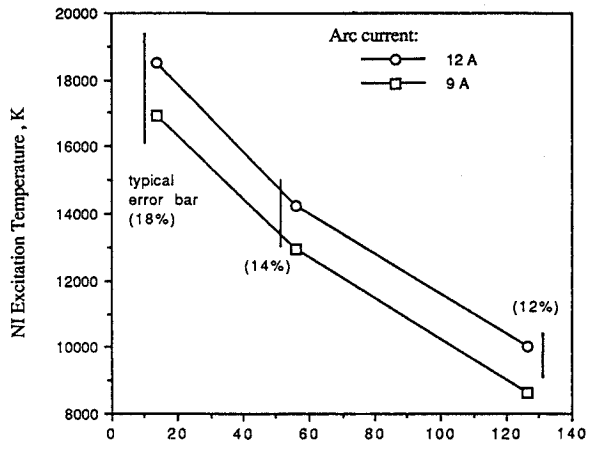

a) Neutral nitrogen excitation temperature

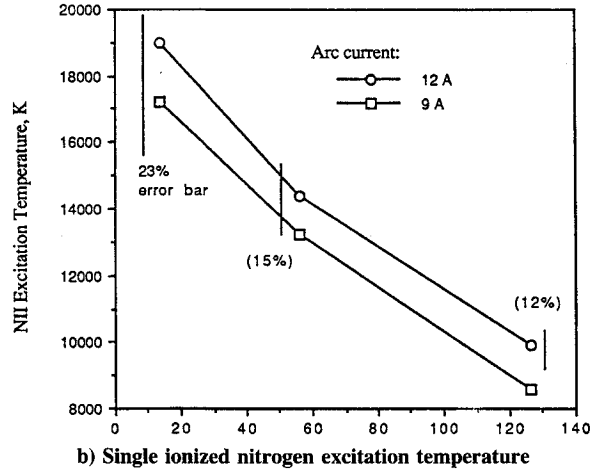

b) Single ionized nitrogen excitation temperature

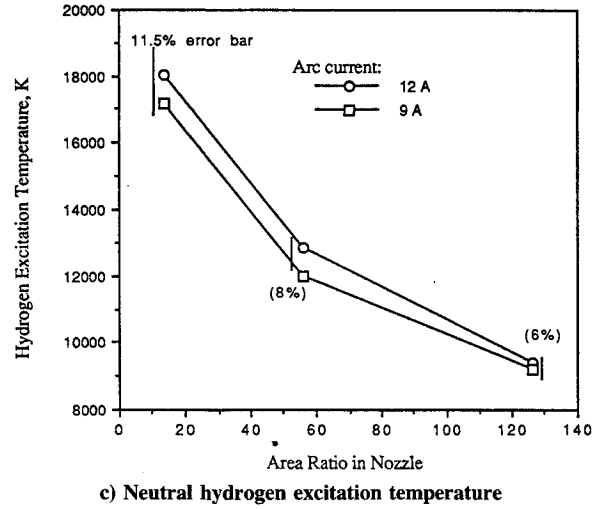

c) Neutral hydrogen excitation temperature

Fig. 3 Electron excitation temperature as a function of area ratio in the nozzle for three plasma species.

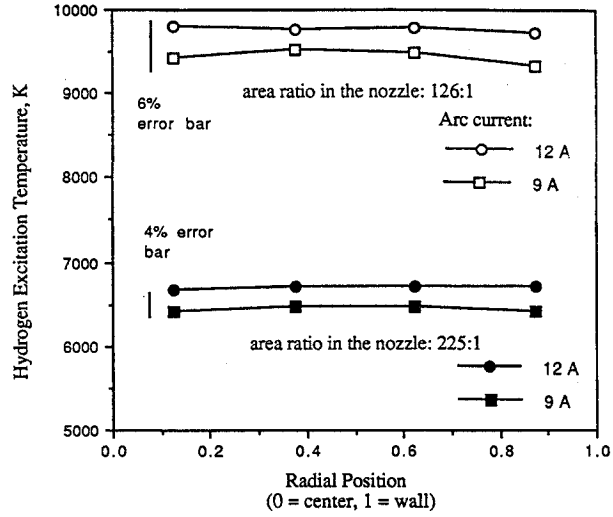

Fig. 4 Neutral hydrogen electron excitation temperature as a function of radial position in the 1:400 nozzles at area ratios 1:127 and 1:225.

the hydrogen excitation temperature did not vary within the inner 87% of the nozzle radius for the 1:400 area expansion ratio nozzle. The temperature measurements at the 1:127 expansion position for the 1:225 expansion nozzle gave nearly the same results for the temperature profiles; the temperature was, within 200 K, identical to the results from the 1:400 expansion nozzle at that location.

The decrease in emission intensity from species other than hydrogen cannot be explained by arguing that these species are depleted at larger radii. Other investigations[7,8] determined no significant variation in species density away from the centerline measured at the exit plane or in the plume behind the nozzle.

Background radiation from the glowing nozzle precluded direct measurements of the free electron temperature from the continuum radiation (free-bound and free-free transition processes). However, several arguments can be introduced to show that the electron temperature was near the atomic excitation temperature. First, there is the close agreement of excitation measurements for NI, NII, and H. Given the different cross sections, radiative rates and densities, it seems unlikely this agreement would occur unless the upper excited state populations were controlled by the same mechanisms of electronic collisional excitation and radiative decay. Second, the energy levels used for the measurements were close to the ionization potentials for the atoms. For example, for NI the measured states were less than 0.6 eV from the continuum. Third, the electron densities measured using Stark broadening were close to the threshold established by Griem[19] (extended by Hey[21]) for partial local thermal equilibrium, a condition for which $T_{ex} = T_e$ (see Discussion).

Molecular Vibration Temperature

The nitrogen vibrational temperature was determined from the intensity ratio of two transitions. According to Herzberg[16] it can be calculated from two molecular bands (denoted subscripts 1 and 2):

$$T_{vib} = \frac{G_1 - G_2}{k \ln(I_2\lambda_2^4 f_1 / I_1\lambda_1^4 f_2)} \tag{2}$$

Only two spectral bands (with their band heads at 380.5 and 375.5 nm) were sufficiently intense and free from overlapping lines or bands to be used for the vibrational temperature determination. Both are $C^3\Pi_u$-$B^3\Pi_g$ transitions in the second positive system of nitrogen. While the absolute oscillator strengths for atomic transitions are reasonably well known

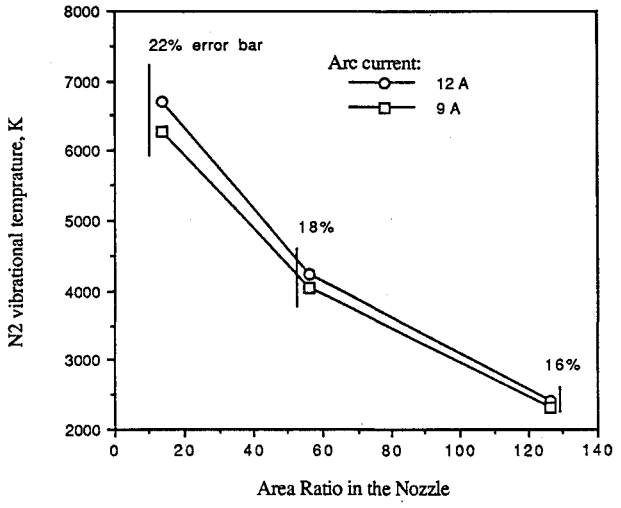

Fig. 5 N_2 Vibrational temperature as a function of area ratio in the 225:1 nozzle.

for most species,[17] only a few have been measured for molecular transitions and the uncertainties even for relative strengths are larger. Thus, the absolute uncertainty of the vibrational temperature determination is rather large (±25%), though trends are accurate within the experimental uncertainty (10%).

Typical vibrational temperature measurements for the 1:225 nozzle at 9 and 12 A are shown in Fig. 5, where it is seen that the temperature decreases from 6500 K near the constrictor to 2500 K at an area ratio of 1:127. While there was a slight dependence on arc current at the upstream end of the nozzle, this disappeared towards the exit plane. Radial profiles could not be measured due to the rapid decrease in spectral intensity at higher radii. Thus, the measured temperatures are only a mean value averaged over the line of sight at the center line.

Rotational Temperature

The intensity ratio method could not be used to determine rotational temperatures because the rotational lines in a molecular band structure are too close together and overlap, precluding the separation of individual lines within one band. To overcome this problem, the theoretical intensity distribution for a band was calculated with an assumed rotational temperature and compared to the measured spectrum. The rotational temperature was found iteratively by varying the temperature of the theoretical distribution, a method used by several authors.[5,22,23] An examination of the observed spectrum led to the selection of the N_2 $C^3\Pi_u$-$B^3\Pi_g$-(1, 4) transition band at 399.8 nm. The equations governing the line intensity and wavelength distributions of the P, Q, and R rotational branches were taken from Herzberg,[16] 50 transitions for each of the branches were included. A simple inverted parabola line shape was used for simulating the lines to reduce computational time. This assumption had little effect where the lines were slightly separated, but introduced substantial errors near the band heads where the lines are positioned closer together.

Figure 6 shows measured and calculated bands for N_2. It is clear that the distribution was well predicted away from the band head at 399.8 nm, but that the agreement at the band head is quite poor. The agreement between measured and calculated spectra, the latter based on a Boltzmann distribution, indicated that the rotational levels were not far from an equilibrium state. The discrepancy at the band head may have been due to the assumed line shape. A recent review with a more accurate line profile improved the results even closer to the band head. Figure 7 shows the rotational temperatures for the 1:225 nozzle at currents of 9 and 12 A determined with this technique. The rotational temperature was found to be higher than the vibrational temperature, and it decreased more rapidly than the vibrational temperature. Note that for T_{rot} the increase in temperature with current level was evident throughout the nozzle.

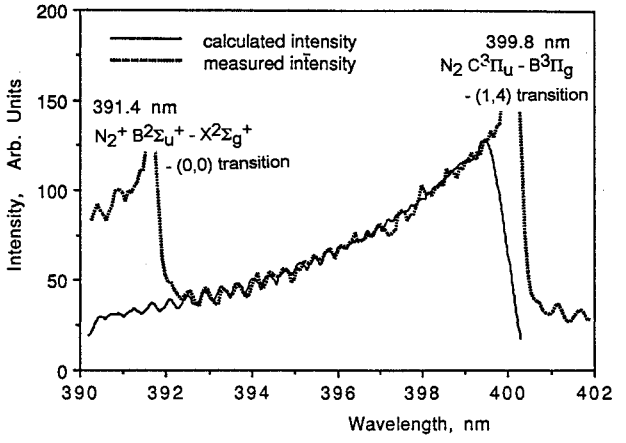

Fig. 6 Typical experimental and calculated N_2 rotational band intensity distributions.

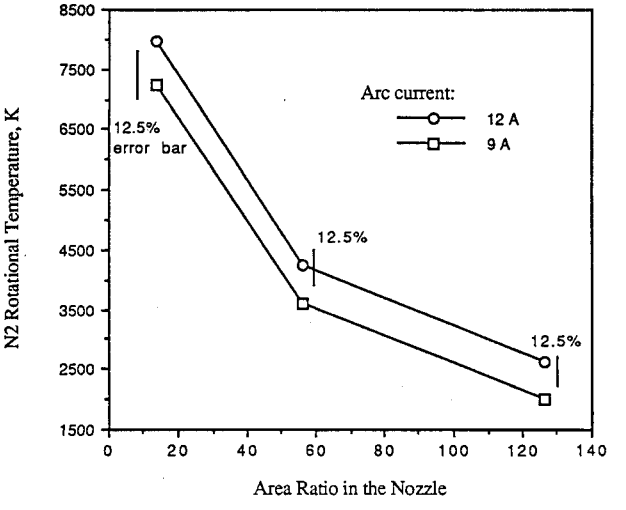

Fig. 7 N_2 Rotational temperature as a function of area ratio in the 225:1 nozzle.

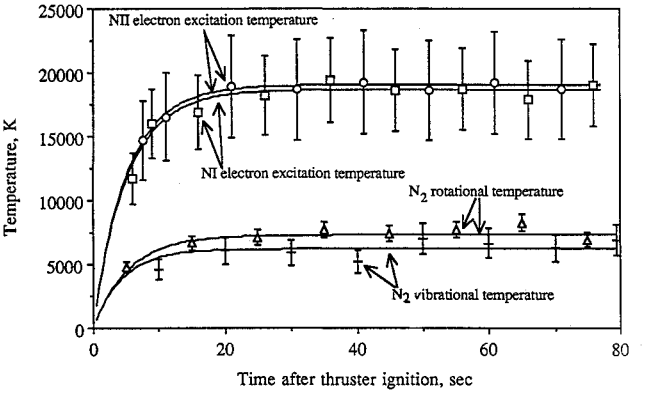

Fig. 8 Time evolution of the plasma temperatures during arcjet startup.

The temporal behavior of the three plasma temperatures was measured in an attempt to establish the importance of wall heat transfer to the plasma characteristics. Shown in Fig. 8 are the mean results from 100 spectra recorded every 0.5–3 s during the startup phase of an arcjet test. The recording

Table 3 Approximate time constants for plasma temperature to reach 63% (=1 − 1/e) of the residual values after thruster ignition

Axial position from constrictor (expansion ratio)	Atomic excitation temperature	Molecular vibration temperature	Molecular rotation temperature
3 mm (1:13.9)	5.0–5.4 s	5.1–5.6 s	4.9–5.6 s
6 mm (1:56.1)	6.9–7.6 s	7.0–7.8 s	7.1–7.7 s
9 mm (1:126.5)	8.1–8.5 s	8.2–9.7 s	8.3–8.6 s

of the spectra was started before thruster ignition to study the startup phase. A curve of the form $T = T_0[1 - \exp(-t/\tau)]$ was used to calculate the desired time constant τ for each plasma temperature. The time constants for the various plasma properties, listed in Table 3, were of the same order for all plasma temperatures. The time constants varied with axial position in the nozzle, ranging from 5 s near the constrictor to 8.5 s near the exit plane. The time constant for the temperature at the outer nozzle wall was approximately 130 s, and the thrust time constant was about 2 s. Given that the current and voltage rise times were <2 s, this result implies that wall heat transfer played only a small role in plasma energy transfer for these operating conditions. It appears, however, that the observed equilibration times result from either thermal or mechanical relaxation of the arcjet components, since the rise times are much longer than acoustic or plasma relaxation rates.

Electron Density

The electron number density was determined from the Stark width of the hydrogen H_β line (486.1 nm).[24] After the full-width at half-maximum (FWHM) for the line had been determined using a Lorentzian fit to the observed profile, the Doppler and Stark broadening contributions were deconvoluted using the results presented by Huddlestone and Leonard.[24] This process required knowledge of the hydrogen kinetic temperature, which was set equal to the measured electron temperature based on relaxation rate calculations presented below.

Typical results, shown in Fig. 9, show that the density decreased from $\approx 10^{21}$ m^{-3} to 2×10^{20} m^{-3} from axial locations at area ratios of 1:14–1:127. While it is obvious that the upstream electron density increased with current level, the downstream density was not sensitive to the arc current. This may be a consequence of the nozzle current distribution.

The radial electron density distribution was measured at an area ratio of 1:127 for both the 1:225 and 1:400 area ratio nozzles. Measurements in the downstream holes for the longer nozzle were precluded by the low electron density and low spectrometer resolution. At the low exit densities line broadening due to the spectrometer instrument function would have contributed to more than 50% of the measured line width. Line profiles were obtained at each radial station and the resulting profiles Abel inverted to obtain the FWHM as a function of radius. The resulting electron density profiles, shown in Fig. 10, are flat. This result, in combination with the excitation temperature measurements, shows that there existed a wide central region with relatively uniform properties. The behavior near the walls could not be detected due to the limited radial resolution. The increased density observed with the longer nozzle may be due to the presence of substantial current density downstream of the measurement point. In other words, the arc current may extend over most of anode length for both the 1:225 and 1:400 nozzles; since these measurements were made at an area ratio of 1:127 for both nozzles, a larger current fraction may extend beyond the measurement point with the longer nozzle than with the shorter one.

The magnitude of these measurements coincides with those made in the thruster plume. The plume measurements shown in Fig. 11 were made using H_β Stark broadening[5] (close to the nozzle) and Langmuir probes.[3,4] While the measurements in the outer plume can be described sufficiently with a $1/x^2$ expansion, the electron density behavior closer to the nozzle shows variations consistent with supersonic flow patterns behind a nozzle.

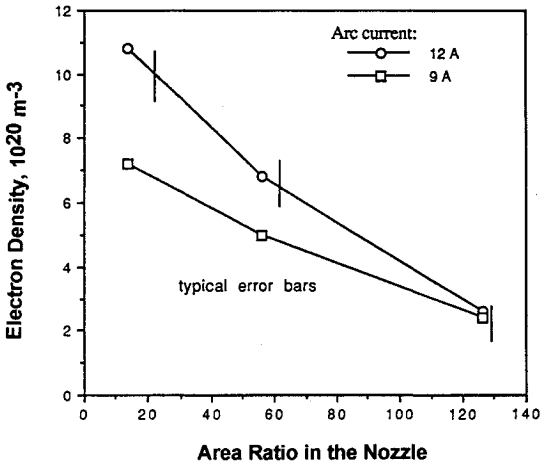

Fig. 9 Electron density as a function of area ratio in the 225:1 nozzle.

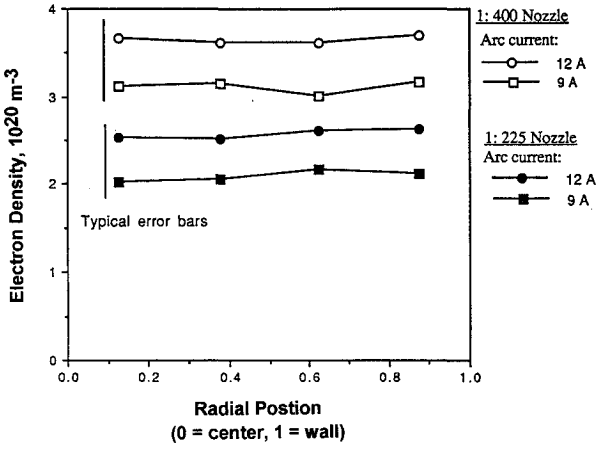

Fig. 10 Electron density as a function of radial position for both the 225:1 and 400:1 nozzles at an area ratio of 126:1.

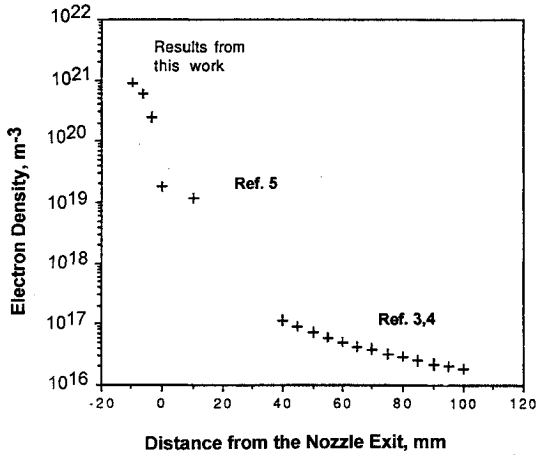

Fig. 11 Comparison of electron density measurements in the arcjet plume with results from this work.

Discussion

The large difference between the atomic excitation, vibrational, and rotational temperatures clearly shows that the plasma

is in a nonequilibrium state throughout the nozzle. The excitation temperature was more than twice as large as either molecular temperature throughout the expansion, and the rotational temperature was higher than the vibrational temperature. Three justifications are presented for equating the excitation temperature to the free electron temperature. First, T_{ex} was the same for the three investigated species. Second, the excited states used in the measurement of the nitrogen species were energetically close to the ionization limit. Third, the states observed and the electron densities satisfied the partial local thermal equilibrium (PLTE) criterion developed by Griem[19] for hydrogen and modified by Hey[21] for nonhydrogenic applications. The criterion demands the dominant collisional depopulation rate from the second to the first energy level in an atom to be 10 times faster than the radiative decay into the ground state. It is written as a lower electron density bound for which the excited state population is controlled by the free electron temperature

$$n_e \geq 2.55 \times 10^{23} \left(\frac{\Delta E}{E_H}\right)^3 \sqrt{\frac{T_e k}{E_H}} \frac{1}{G_{\text{eff}}} \text{ m}^{-3} \qquad (3)$$

where the factors G_{eff} were obtained from van Regemorter.[25] This criterion established a lower bound of $\approx 10^{21}$ m^{-3} for the 18,000 K temperature near the constrictor and 8×10^{21} m^{-3} for the 7000 K temperature near the exit plane. Thus, based on this PLTE criterion, equating the excitation temperature to the free electron temperature is acceptable near the constrictor but unjustified near the exit plane. However, Skorupski and Suckewer,[26] have shown that heavy particle elastic collisions can dramatically relieve the electron density requirements for PLTE, because they accelerate the equilibration process. This coupled with the first two arguments above indicate that setting $T_{ex} = T_e$ was a reasonable approximation. Even the temperatures measured from H_α and H_β should not deviate much from these values, although the temperatures measured from electron transitions from lower energy levels tend to overestimate the excitation temperatures found from higher energy levels in the case of "terminal nonequilibrium."[27] This condition, however, is far from being fulfilled and the excitation temperatures for all three considered species should be close together.

Several plasma relaxation rates were evaluated to establish which processes played a dominant role in the plasma expansion. These relaxation rates represent the time it takes for a particle with an equilibrium condition$_1$ to reach a new equilibrium condition$_2$. They are calculated by dividing the energy difference of the two conditions by the initial energy exchange rate for this collision. They should be compared with the average particle residence time in the nozzle, which was conservatively estimated to be $\approx 5 \times 10^{-6}$ s by dividing the nozzle length by one-half of the average exhaust velocity. The latter was estimated from the measured thruster specific impulse. The plasma relaxation times, summarized in Table 4, were calculated using the temperature and density measurements presented above and relations from Vincenti and Kruger[28] and Venugopalan.[29] For example, the energy equilibration

Table 4 Relaxation times in the arcjet nozzle plasma

Time, s	Process
10^{-10}–10^{-11}	Electron self relaxation[28]
10^{-9}	Hydrogen-hydrogen (or proton) kinetic relaxation[28]
10^{-8}	Electron-proton kinetic relaxation[28]
10^{-7}	Direct electron-hydrogen relaxation (table in Ref. 28)
10^{-6}–10^{-7}	N_2 Rotational relaxation[27]
10^{-6}	Hydrogen-N_2 kinetic relaxation[28]
$\geq 10^{-6}$	Average particle residence time in the nozzle
10^{-6}–10^{-4}	N_2 Vibrational relaxation[27]

times between the observed plasma species were used to establish the atomic hydrogen kinetic temperature. This relaxation time is given by Venugopalan[29] (p. 144, Eq. 215, densities in cm^{-3}, cross sections in cm^{-2})

$$t_{1-2} = 1.3 \times 10^{-5} \frac{(M_1 + M_2)^2}{n_2 M_1 M_2^{1/2} \langle \sigma_{1-2}(T_2) \rangle T_2^{1/2}} \text{ s} \qquad (4)$$

where the subscripts refer to the species in question, was used to compare the H atom-N_2 relaxation and the H atom-electron relaxation.[30] In these estimates the N_2 kinetic temperature was assumed to be equal to the measured rotational temperature (justified by Vincenti and Kruger[28]) and the N_2 density was set to $\approx 10^{22}$ m^{-3} based on propellant flow rate, nozzle area, and exhaust velocity. The momentum transfer cross section for these H-N_2 collisions is not known, so it was estimated from the geometric particle radii.[31] The cross section for electron-hydrogen collisions was obtained from Mitchner and Kruger.[30] The results, relaxation times of 10^{-7} s for electron-hydrogen collisions and 2×10^{-6} s for N_2-H collisions, could not be used to conclusively establish an estimate for the hydrogen kinetic temperature. However, when the relaxation times were calculated for the two-step process, electron-proton and proton-atomic hydrogen collisions, the results were more significant. The large Coulomb cross section for the electron-proton interaction gives a relaxation time relation of (Venugopalan,[29] p. 154, Eq. 232, density in m^{-3})

$$t_{\text{eq}}^{e-p} \approx 2.5 \times 10^8 \frac{T_e^{3/2}}{n_e \ln \Lambda} \text{ s} \qquad (5)$$

which, for the measured conditions, yields a relaxation time of 10^{-8} s. In Ref. 28, Table 11 yields a time of 10^{-9} s for the atomic hydrogen-proton relaxation. Thus, the two-step process, consisting of an electron-proton collision followed by a proton-neutral hydrogen collision, is two orders of magnitude faster than the single step hydrogen atom-nitrogen molecule collision process. This led to the use of the electron excitation temperature as a rough estimate for the kinetic hydrogen temperature when the Doppler broadening was calculated for the determination of the electron density from the Stark effect. Similar two-step processes were investigated to check additional processes (electron-NII, NII-H and N_2-N, N-H), but they were found to be slower than the process described above. This is a result of the large mass difference between hydrogen atoms and nitrogen molecules (1:28), which slows this process, and the fast relaxation between electrons and protons due to the large Coulomb cross section.

While the measured rotational and vibrational temperatures were about the same near the exit plane, the rotational temperature appeared to be slightly higher close to the constrictor (Fig. 7). The observed difference in the behavior of the two temperatures during the expansion may result from the different relaxation times for these processes. The rotational relaxation is "somewhat slower"[28] than the translational relaxation. With Eq. (4) the translational relaxation was calculated to be 10^{-7} s, so the rotational relaxation should have a time constant of 10^{-6}–10^{-7} s. The vibrational relaxation was calculated from (Vincenti and Kruger,[28] p. 204, Eq. 2.13a)

$$\tau = C \frac{e^{(K_2/T)^{1/3}}}{p} \qquad (6)$$

where the temperature T is in Kelvin and the pressure p in MPa. The constants C and K_2 depend on the gas, for nitrogen $K_2 = 1.91 \times 10^6$ K and $C = 7.12 \times 10^{-10}$ s MPa. The shortest possible time constant results from using the propellant feed pressure (0.8–1 MPa) in Eq. (6), which results in a time constant of 10^{-6} s. Of course, during the expansion this value

will increase by three orders of magnitude, so that the vibrational relaxation times are the longest time constants for the nozzle plasma. The difference in the time constants for rotation and vibration would explain the difference in the slope for the two temperatures.

Conclusion

The spectroscopic analysis of the light emitted from the plasma inside the nozzle of a 1-kW class arcjet thruster operated on a 2:1 hydrogen-nitrogen mixture showed the expected atomic and molecular nitrogen and hydrogen spectral lines. In addition, considerable NH and small traces of NH_2 and tungsten, eroded from the electrodes, were found. Measurements of excitation, vibrational, and rotational temperatures proved the plasma to be in a nonequilibrium state throughout the nozzle. It appears that the excited upper atomic states can be described using a PLTE model, though this should be investigated more carefully for the plasma near the exit plane. A collisional-radiative model, allowing for a minimum of two fluid temperatures, will be required to accurately model the arcjet plasma expansion. The atomic excitation temperature was found to drop from 18,000 to 9000 K during the expansion, and the molecular temperatures were found to be considerably lower, ranging from 6500 to 3000 K for the vibrational and 8000 to 3000 K for the rotational temperatures, respectively. The electron density dropped from $\approx 10^{21}$ m^{-3} near the constrictor to 2×10^{20} m^{-3} near the exit, and was sensitive to the arc current only near the constrictor. Radial profiles of the excitation temperature and electron density showed that both were flat over the observed inner 87% of the nozzle radius. This indicated the presence of a broad, uniform central region with low gradients, probably surrounded by high-temperature gradients close to the wall. The relaxation times calculated for the plasma conditions qualitatively explain the different temperature trends.

References

[1]Jahn, R. G., *Physics of Electric Propulsion*, 1st ed., McGraw-Hill, New York, 1968.

[2]Curran, F. M., Manzella, D. H., and Pencil, E. J., "Performance Characterization of a Segmented Anode Arcjet Thruster," AIAA Paper 90-2582, July 1990.

[3]Carney, L. M., "An Experimental Investigation of an Arcjet Exhaust Using Langmuir Probes," NASA TM 102346, Dec. 1988.

[4]Sankovic, J., "Investigations of the Arcjet Plume Near Field Using Electrostatic Probes," NASA TM 103638, Oct. 1990.

[5]Manzella, D. H., Curran, F. M., Myers, R. M., and Zube, D. M., "Preliminary Plume Characteristics of an Arcjet Thruster," AIAA Paper 90-2645, July 1990.

[6]Keefer, D., Gogel, T., Sedghinasab, A., and Ruyten, W. M., "Laser Fluorescence Velocimetry of an Arcjet Exhaust Plume," International Electric Propulsion Conf., Paper 91-093, Viareggio, Italy, Oct. 1991.

[7]Capelli, M. A., Hanson, R. K., Liebeskind, J. G., and Manzella, D. H., "Optical Diagnostics of a Low Power Hydrogen Arcjet," International Electric Propulsion Conf., Paper 91-091, Viareggio, Italy, Oct. 1991.

[8]Cohen, R. B., "Optical Diagnostics of Hydrogen Arcjets," International Electric Propulsion Conf., Paper 91-095, Viareggio, Italy, Oct. 1991.

[9]Janson, S. W., Welle, R. P., Schulthess, D. R., and Cohen, R. B., "Arcjet Plume Characterization, Part II: Optical Diagnostic Analysis," AIAA Paper 90-2643, July 1990.

[10]Curran, F. M., private communication, NASA Lewis Research Center, Cleveland, OH, May 1991.

[11]Ishii, M., and Kuriki, K., "Optical and Analytical Studies of Arc Column in DC Arcjet," AIAA Paper 87-1086, May 1987.

[12]Curran, F. M., and Haag, T. W., "An Extended Life and Performance Test of a Low Power Arcjet," AIAA Paper 88-3106, July 1988.

[13]Gruber, R. P., "Power Electronics for an 1-kW Arcjet Thruster," AIAA Paper 86-1507, July 1986.

[14]Zube, D. M., and Myers, R. M., "Techniques for Spectroscopic Measurements in an Arcjet Nozzle," *Journal of Propulsion and Power*, Vol. 8, No. 1, 1992, pp. 254–256.

[15]Bronstein, I. N., and Semendjajew, K. A., *Taschenbuch der Mathematik*, 21st ed., B. G. Teubner Verlagsgesellschaft, Leipzig, Germany, 1979.

[16]Herzberg, G., *Molecular Spectra and Molecular Structure, I. Spectra of Diatomic Molecules*, D. van Nostrand Co., New York, 1959.

[17]Reader, J., Corliss, C. H., Wiese, W. L., and Martin, G. A., *Wavelengths and Transition Probabilities for Atoms and Atomic Ions, Part I: Wavelength, Part II: Transition Probabilities*, National Bureau of Standards, Washington, DC, 1980.

[18]Pearse, R., and Gaydon, A., *The Identification of Molecular Spectra*, 2nd ed., Wiley, New York, 1950.

[19]Griem, H. R., *Plasma Spectroscopy*, 1st ed., McGraw-Hill, New York, 1964.

[20]Lochte-Holtgreven, W., *Plasma Diagnostics*, North Holland, Amsterdam, 1968.

[21]Hey, J. D., "Criteria for Local Thermal Equilibrium in Non-Hydrogenic Plasmas," *Journal for Quantitative Spectroscopy and Radiative Transfer*, Vol. 16, No. 1, 1976, pp. 69–75.

[22]Piper, L. G., Holtzclaw, K. W., and Green, B. D., "Experimental Determination of Einstein Coefficients for the N_2 (B-A) Transition," *Journal of Chemical Physics*, Vol. 90, No. 10, 1989, pp. 5337–5345.

[23]Beylich, A. E., "Experimental Investigation of Carbon Dioxide Jet Plumes," *Physics of Fluids*, Vol. 14, No. 5, 1971, pp. 898–905.

[24]Huddlestone, R. H., and Leonard, S. L., *Plasma Diagnostic Techniques*, 1st ed., Academic Press, New York, 1965.

[25]Regemorter, H. v., "Rate Collisional Excitation in Stellar Atmospheres," *Astrophysical Journal*, Vol. 136, No. 3, 1962, pp. 906–915.

[26]Skorupski, A., and Suckewer, S., "Nonthermal Equilibrium Parameters of Weakly Ionized Plasma," *Journal of Physics B: Atomic and Molecular Physics*, Vol. 7, No. 11, 1974, pp. 1401–1410.

[27]Park, C., "Hydrogen Line Ratios as Electron Temperature Indicators in Nonequilibrium Plasmas," *Journal for Quantitative Spectroscopy and Radiative Transfer*, Vol. 12, No. 2, 1972, pp. 323–370.

[28]Vincenti, W. G., and Kruger, C. H., *Introduction of Physical Gas Dynamics*, Robert E. Krieger Publishing, New York, 1967.

[29]Venugopalan, M., *Reactions Under Plasma Conditions*, 1st ed., Wiley Interscience, New York, 1965.

[30]Mitchner, M., and Kruger, C., *Partially Ionized Plasmas*, 1st ed., Wiley Interscience, New York, 1973.

[31]Weast, R. C., *CRC Handbook of Chemistry and Physics*, 53rd ed., CRC Press, Cleveland, OH, 1972.